Available online at www.eccomasproceedia.org
Eccomas Proceedia COMPDYN (2023) 4306-4318

ECCOMAS
Proceedia

COMPDYN 2023
9th ECCOMAS Thematic Conference on
Computational Methods in Structural Dynamics and Earthquake Engineering
M. Papadrakakis, M. Fragiadakis (eds.)
Athens, Greece, 12-14 June 2023

STEADY-STATE RESPONSE OF A HIGH-STRENGTH MOMENT-RESISTING STEEL FRAME-SELF-CENTERING STEEL PLATE SHEAR WALL SYSTEM

Chuandong Xie[1], Xiantie Wang[1], and George Vasdravellis[2]

[1]School of Civil Engineering, Xi'an University of Architecture and Technology, Xi'an, 710055, China
e-mail: {chuandongxie,wangxtgm}@xauat.edu.cn

[2] School of Energy, Geoscience, Infrastructure and Society, Institute for Infrastructure & Envi-ronment, Heriot-Watt University, Edinburgh, EH14 4AS, UK
e-mail: G.Vasdravellis@hw.ac.uk

Abstract. *A resilient system comprised of a high-strength moment-resisting steel frame (HS-MRF) and self-centering steel plate shear walls (SC-SPSWs) has been proposed to address the issue of frame expansion. The system's steady-state dynamic responses were analysed using an analytical solution of a single-degree-of-freedom nonlinear oscillator under harmonic excitation, solved via the method of slowly varying parameters. A stability analysis was also conducted to assess the behaviour of singular points. The hysteretic model for the proposed structure is a combination of validated bilinear, self-centering, and pinching hysteresis, representing the high-strength frame, self-centering frame, and steel plate shear wall, respectively. The results indicate that increasing the proportion of bilinear hysteresis has minimal impact on resonance but can decrease nonlinearity for lower excitation intensities. However, for higher intensities, increasing the bilinear hysteresis can significantly decrease peak responses and reduce both the jump and unbounded phenomena. Most of the unstable responses can be divided into four zones, and the unstable regions are greatly influenced by the ratio of hysteretic models. This steady-state dynamic analysis suggests that a well-designed mixture of high-strength moment-resisting steel frames and self-centering steel plate shear walls can bring a favourable seismic performance.*

Keywords: Resilient structure, Nonlinear dynamics, Frequency response, Stability analysis, Frame-wall system

ISSN:2623-3347
Peer-review under responsibility of the organizing committee of COMPDYN 2023.
doi: 10.7712/120123.10720.21000

1 INTRODUCTION

Recent developed self-centering structural systems are designed to manage the structural damage through the introduction of the rocking connections, easy-to-replace energy-dissipating elements and post-tensioned (PT) system. During a strong earthquake, gap openings occurs in the rocking connections, elongating the PT elements which provides the restoring force and brings the buildings back to their origin position. The energy is dissipated by the elements that are across the rocking connections and will be replaced after the earthquake [1–4]. However, the frame will expand due to the elongation of the beams since the beam rotate at their flanges, and the expansion beyond a certain level can induce failure in the perimeter self-centering frame and excessive cracks in the slabs [5,6]. As an alternative solution, an innovative dual frame-wall resilient system consisting of a high-strength moment-resisting steel frame (HS-MRF) and self-centering steel plate shear walls (SC-SPSWs) is proposed [7], as shown in Fig. 1. The HS-MRF provide large elastic deformation capability due to the use of high-strength steel (e.g. Q460), and all the SC-SPSWs are located at the outside bays and use composite columns, steel beams, steel plates, PT strands in the beams and PT bars in the columns. The steel plates serve as energy-dissipating elements and are connected to the boundary elements by bolt work, so that the plates are easy to replace. The slot connections between HS-MRF and SC-SPSWs allow frame expansion and enable the continuous slab free from damage. Four performance levels are designed, including immediate occupancy (IO), damage control (DC), life safety (LS) and collapse prevention (CP), corresponding to the peak inter-storey drifts of 0.4%, 1.0%, 2.0% and 4.0%, respectively. The HS-MRF work provides larger resistance to lateral forces but remains elastic during both IO and DC levels, and the SC-SPSW ensures recentering capability at the DC level by using the PT elements. More details can be found in the previous paper [7].

Experimental and numerical studies have effectively characterized the mechanical behaviour and dynamic responses of self-centering systems, as evidenced by recent research [8–11]. However, obtaining a complete picture can be both time-consuming and costly, and the results are often not continuous. To overcome these limitations, the steady-state analysis of the system under harmonic motion can explore suitable designs and perform parameter investigations, optimizations, and statistical model updating. Nonetheless, obtaining closed-form solutions for the dynamic response of the systems is a challenging task due to the continuous but non-differentiable properties of hysteretic models. This can be solved by the method of averaging, which has been implemented into flag-shaped hysteresis [12] and flag-shaped hysteresis with viscous damping [13]. For the self-centering systems without considering damping, Christopoulos (2004) [12] finds that both stable solution branches can be achieved depending on the nature of the excitation, and an amplitude jump phenomenon is also found when increasing frequency and decreasing frequency sweeps. Kitayama and Yang (2021) [13], considering the self-centering hysteresis with viscous damping, and with or without elasto-plastic hysteresis, finds that the self-centering systems may have large displacement demand due to the potentially limited energy dissipation. However, the performance levels in the dual frame-wall resistant system present a complicated task to determine the resonant responses. At the IO level, the energy is absorbed by viscous damping only, but by viscous damping and infill web plate which exhibits pinching behaviour at the DC level. While at the LS level, more energy is dissipated by the HS-MRF and the web plate will fail, and then at the CP level the energy is mainly absorbed by the HS-MRF. Therefore, more research is required to address the issue of resonant responses of the proposed dual frame-wall system.

To this end, this paper first summarised the hysteresis and proposed the analytical expressions

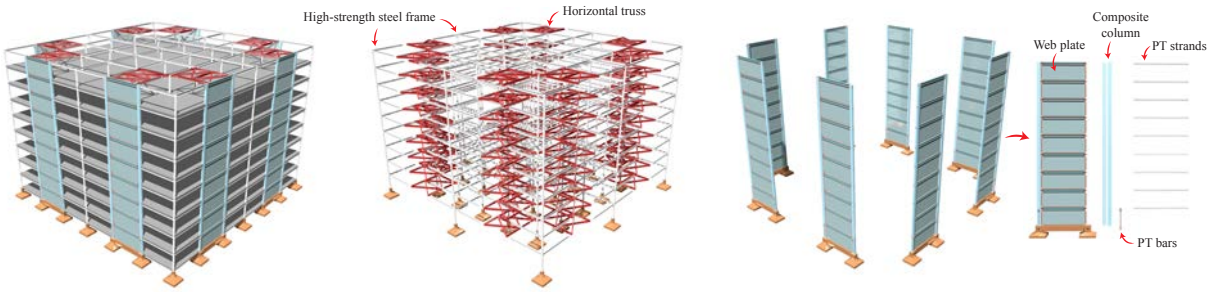

(a) frame-wall system (b) HS-MRF (c) SC-SPSWs

Figure 1: Dual frame-wall resilient system [7]

for the steady-state response and the corresponding stability of a nonlinear oscillator subjected to harmonic excitation considering viscous damping, followed by the discussion of dynamic behaviour of the dual frame-wall system. The findings shed light on the inherent dynamic properties of the dual frame-wall system and suggest that a reasonable combination can achieve a favourable seismic performance. This research is based on previous work [**?**] where more details can be found.

2 HYSTERETIC MODELS

The proposed dual frame-wall system consists of a HS-MRF and SC-SPSWs. Due to the use of high-strength material, the HS-MRF can keep elastic up to the LS level, and then present beam-hinge ductile response [14]. Recently developed hinge techniques that are easy to replace [15–17] can also be employed. All these studies show that the HS-MRF exhibit bilinear hysteretic responses. Fig. 2a shows the bilinear hysteresis, where k_{iH}, f_{yH} and α_{H} are the initial stiffness, yielding strength and post-yielding stiffness ratio of the model, respectively. The SC-SPSW is composed of a pure self-centering frame and infill-thin web plates, as shown in Fig. 1c. During IO level, the system work elastically. After that, the interfaces in the rocking connection detach, elongating the PT elements and the energy is dissipated by the infill-thin web plates. Available investigations on self-centering frame [5, 7, 18–21] show that the prestressed design provides recentering ability, and the pure self-centering frame exhibit trilinear hysteretic relationship. Studies on the infill-thin web plates [22–25] also find that due to the buckling and plastic deformation, the shear plate shows pinching effect in hysteretic curves. Since the coupling effect between thin web plates and self-centering frame are negligible, the hysteretic behaviour of SC-SPSW is assumed by a trilinear relationship superposed by a pinching relationship. Fig. 2b shows the hysteretic model of self-centering system, where k_{iS}, f_{yS} and α_{S} are the initial stiffness, yielding strength and decompressed stiffness ratio of the model, respectively. Fig. 2c shows the hysteretic model of web plate, which is modified from Pinching 4 material [26]. The model consists of response envelopes (m path), unload-reload paths (p and n path) and damage rules. Details of the first and third rules can be found in [26]. Since the kinematic hardening plays a domain role in thin web plate, and in order to be compatible with bilinear hysteresis, the pinching rules are modified from the previous study [26], as shown in Fig. 2d. The unloading-reloading rule is defined by unloading and reloading points. Taking the positive-negative branch as example, n_{u} is defined from $n_{\mathrm{u},0}$ and $n_{\mathrm{u},1}$ by a parameter β_{uf}, and n_{r} is defined by two parameters, β_{rd} and β_{rf}, which control the displacement and force portion, respectively. The modified pinching hysteresis has been implemented in OpenSees [27] as an uniaxial material, named Pinching4M.

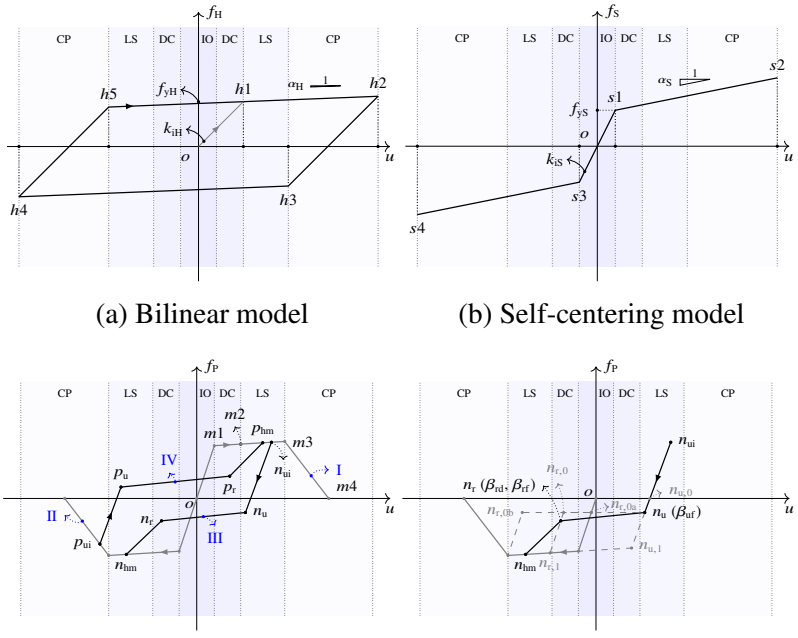

(a) Bilinear model (b) Self-centering model

(c) Pinching model (d) Pinching rulel

Figure 2: Hysteretic models

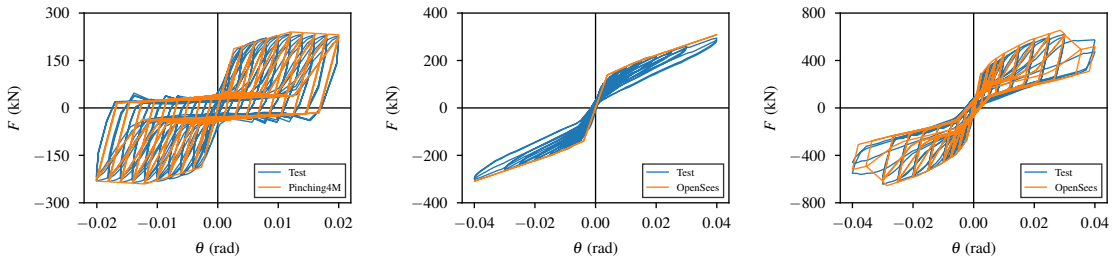

(a) Pinching hysteresis [24] (b) Self-centering hysteresis [7] (c) SC-SPSW [7]

Figure 3: Verification of hysteretic models

The validation of pinching and self-centering hysteresis is shown in Fig. 3a, based on the experiment carried by Yu et al. (2011) [24], and it is found that the modified pinching hysteresis can well predict the hysteretic responses. The self-centering hysteresis and SC-SPSW model are verified through the specimens of SC-SPSW-1 and SC-SPSW-4 in Reference [7]. Again both hysteretic responses can be well matched by the self-centering hysteresis and the combination of self-centering and pinching hysteresis, respectively.

3 HARMONIC FREQUENCY RESPONSE

3.1 Derivation of closed-form frequency response

The equation of a general nonlinear single-degree-of-freedom oscillator subjected to a steady harmonic excitation can be written as

$$m\frac{\mathrm{d}^2u(t)}{\mathrm{d}t^2}+c\frac{\mathrm{d}u(t)}{\mathrm{d}t}+k\bar{f}(u)=-mA_{\mathrm{g}}\cos\omega_{\mathrm{g}}t \tag{1}$$

where m is the mass; $u(t)$ is the relative displacement; c is the damping constant; k is the initial stiffness of structure; $\bar{f}(u)$ is normalised restoring force; A_{g} and ω_{g} are amplitude and the circular frequency of the base excitation, respectively.

Let

$$\omega_0 = \sqrt{\frac{k}{m}}; \qquad \tau = \omega_0 t; \qquad \zeta = \frac{c}{2m\omega_0}; \qquad \sigma = \frac{\omega_{\mathrm{g}}}{\omega_0}; \qquad u_{\mathrm{s}} = -\frac{mA_{\mathrm{g}}}{k} \tag{2}$$

where ω_0 is the initial natural circular frequency of the system; τ is the nondimensional time; ζ is the damping ratio; σ is the excitation frequency ratio.

Eq. (1) can be written as

$$\frac{\mathrm{d}^2 u}{\mathrm{d}\tau^2} + 2\zeta\frac{\mathrm{d}u}{\mathrm{d}\tau} + \bar{f}(u) = u_{\mathrm{s}}\cos\sigma\tau \tag{3}$$

Assuming that the steady-state response of the system exists, the solution of Eq. (3) can be written as

$$u(\tau) = a\cos(\sigma\tau + \beta) \tag{4}$$

where a and β are slowly varying parameters. Letting $\theta = \sigma\tau + \beta$ and using the method of averaging [28], we have

$$-2\zeta\sigma a_0 + S(a_0) = u_{\mathrm{s}}\sin\beta_0 \tag{5}$$

$$-\sigma^2 a_0 + C(a_0) = u_{\mathrm{s}}\cos\beta_0 \tag{6}$$

in which

$$S(a) = \frac{1}{\pi}\int_0^{2\pi} \bar{f}(a\cos\theta)\sin\theta\mathrm{d}\theta \tag{7}$$

$$C(a) = \frac{1}{\pi}\int_0^{2\pi} \bar{f}(a\cos\theta)\cos\theta\mathrm{d}\theta \tag{8}$$

and a_0 and β_0 are the amplitude and the phase during steady-state response, respectively. Let

$$\bar{S} = \frac{S(a_0)}{a_0}; \qquad \bar{C} = \frac{C(a_0)}{a_0} \tag{9}$$

Substituting Eq. (9) for Eqs. (5) and (6), squaring each equation and summing them, we obtain

$$R_{\mathrm{u}} - \frac{R_{\mathrm{a}}}{\sqrt{\left(\bar{S} - 2\zeta\sigma\right)^2 + \left(\bar{C} - \sigma^2\right)^2}} = 0 \tag{10}$$

in which

$$R_{\mathrm{u}} = \frac{a_0}{u_{\mathrm{s}}}; \qquad R_{\mathrm{a}} = \frac{A_{\mathrm{g}}}{A_{\mathrm{s}}}; \qquad A_{\mathrm{s}} = \frac{ku_{\mathrm{y}}}{m} \tag{11}$$

where R_{u} is the normalised amplitude response; R_{a} is the normalised excitation.

Noting that no specific hysteresis has been taken into account, Eq. (10) can be applied for the non-time sensitive nonlinear structural systems.

3.2 Derivation of stability

The stability of the different portions of the response curves can be identified by investigating the nature of the singular points of Eq. (10). Let

$$a = a_0 + \mu_0 e^{\lambda t}; \qquad \beta = \beta_0 + \nu_0 e^{\lambda t} \tag{12}$$

where μ, ν are constants.

Considering the results of frequency response, we have

$$\begin{bmatrix} -2\sigma\lambda + \frac{\partial S}{\partial a} - 2\zeta\sigma & \sigma^2 a_0 - C(a_0) \\ \frac{\partial C}{\partial a} - \sigma^2 & S(a_0) - 2\sigma a_0 \lambda - 2\zeta\sigma a_0 \end{bmatrix} \begin{bmatrix} \mu_0 \\ \nu_0 \end{bmatrix} = \begin{bmatrix} 0 \\ 0 \end{bmatrix} \tag{13}$$

Taking the determinant of Eq. (13) gives the following

$$(2\sigma\lambda)^2 + 2\sigma\lambda P + Q = 0 \tag{14}$$

where

$$P = 4\zeta\sigma - \bar{S} - \frac{\partial S}{\partial a} \tag{15}$$

$$Q = \left(\bar{C} - \sigma^2\right)\left(\frac{\partial C}{\partial a} - \sigma^2\right) + 2\zeta\sigma\left(2\zeta\sigma - \frac{\partial S}{\partial a} - \bar{S}\right) + \frac{\partial S}{\partial a}\bar{S} \tag{16}$$

The solutions for Eq. (14) are

$$\lambda_{1,2} = \frac{-P \pm \sqrt{P^2 - 4Q}}{4\sigma} \tag{17}$$

The stability of singular points depends on the sign of solutions, which can be determined by the sign of P and Q. Reference [28] shows that only when both $P > 0$ and $Q > 0$, the singular points are stable. Noting that no hysteresis is specified in Eq. (14), again the conclusion can be used for non-time sensitive nonlinear structural systems.

3.3 Dual frame-wall system

For the dual frame-wall resilience system, the $\bar{f}(u)$ can be written as

$$\bar{f}(u) = \bar{f}(u)_{\mathrm{H}} + \bar{f}(u)_{\mathrm{S}} + \bar{f}(u)_{\mathrm{W}} \tag{18}$$

where $\bar{f}(u)_{\mathrm{H}}$, $\bar{f}(u)_{\mathrm{S}}$ and $\bar{f}(u)_{\mathrm{W}}$ are the normalised restoring force of bilinear, self-centering and pinching hysteretic models and can be calculated by Eqs. (19) to (21), respectively.

$$\bar{f}_{\mathrm{H}}(u) = \begin{cases} \bar{f}_{\mathrm{H1}} = \bar{k}_{\mathrm{iH}}\left(u - (1-\alpha_{\mathrm{H}})\left(a - u_{\mathrm{yH}}\right)\right) & u \in (u_{\mathrm{H1}}, u_{\mathrm{H2}}) \quad (19a) \\ \bar{f}_{\mathrm{H2}} = \bar{k}_{\mathrm{iH}}\left(\alpha_{\mathrm{H}} u - u_{\mathrm{yH}}\left(1-\alpha_{\mathrm{H}}\right)\right) & u \in (u_{\mathrm{H2}}, u_{\mathrm{H3}}) \quad (19b) \\ \bar{f}_{\mathrm{H3}} = \bar{k}_{\mathrm{iH}}\left(u + (1-\alpha_{\mathrm{H}})\left(a - u_{\mathrm{yH}}\right)\right) & u \in (u_{\mathrm{H3}}, u_{\mathrm{H4}}) \quad (19c) \\ \bar{f}_{\mathrm{H4}} = \bar{k}_{\mathrm{iH}}\left(\alpha_{\mathrm{H}} u + u_{\mathrm{yH}}\left(1-\alpha_{\mathrm{H}}\right)\right) & u \in (u_{\mathrm{H3}}, u_{\mathrm{H4}}) \quad (19d) \end{cases}$$

$$\bar{f}_{\mathrm{S}}(u) = \begin{cases} \bar{f}_{\mathrm{S1}} = \bar{k}_{\mathrm{iS}}\left(\alpha_{\mathrm{S}} u + u_{\mathrm{y}}\left(1-\alpha_{\mathrm{S}}\right)\right) & u \in (u_{\mathrm{S1}}, u_{\mathrm{S2}}) \quad (20a) \\ \bar{f}_{\mathrm{S2}} = \bar{k}_{\mathrm{iS}} u & u \in (u_{\mathrm{S2}}, u_{\mathrm{S3}}) \quad (20b) \\ \bar{f}_{\mathrm{S3}} = \bar{k}_{\mathrm{iS}}\left(\alpha_{\mathrm{S}} u - u_{\mathrm{y}}\left(1-\alpha_{\mathrm{S}}\right)\right) & u \in (u_{\mathrm{S3}}, u_{\mathrm{S4}}) \quad (20c) \end{cases}$$

$$\bar{f}_{\mathrm{W}}(u)=\begin{cases}\bar{f}_{\mathrm{W1}}=\bar{k}_{\mathrm{iW}}\left(u+\left(1-\alpha_{\mathrm{W}}\right)\left(u_{\mathrm{y}}-a\right)\right) & u\in\left(u_{\mathrm{W1}},u_{\mathrm{W2}}\right) \quad (21a)\\ \bar{f}_{\mathrm{W2}}=\bar{k}_{\mathrm{iW}}\dfrac{\left(\beta_{\mathrm{uf}}-\beta_{\mathrm{rf}}\right)u+\beta_{\mathrm{rf}}\gamma_2+\beta_{\mathrm{rd}}\beta_{\mathrm{uf}}a}{\gamma_2+a\beta_{\mathrm{rd}}} & u\in\left(u_{\mathrm{W2}},u_{\mathrm{W3}}\right) \quad (21b)\\ \bar{f}_{\mathrm{W3}}=\bar{k}_{\mathrm{iW}}\dfrac{\left(\frac{1-\beta_{\mathrm{rf}}}{a}u+\beta_{\mathrm{rd}}-\beta_{\mathrm{rf}}\right)\gamma_1}{1-\beta_{\mathrm{rd}}} & u\in\left(u_{\mathrm{W3}},u_{\mathrm{W4}}\right) \quad (21c)\\ \bar{f}_{\mathrm{W4}}=\bar{k}_{\mathrm{iW}}\left(u-\left(1-\alpha_{\mathrm{W}}\right)\left(u_{\mathrm{y}}-a\right)\right) & u\in\left(u_{\mathrm{W4}},u_{\mathrm{W5}}\right) \quad (21d)\\ \bar{f}_{\mathrm{W5}}=\bar{k}_{\mathrm{iW}}\dfrac{\left(\beta_{\mathrm{uf}}-\beta_{\mathrm{rf}}\right)u-\beta_{\mathrm{rf}}\gamma_2-\beta_{\mathrm{rd}}\beta_{\mathrm{uf}}a}{\gamma_2+a\beta_{\mathrm{rd}}} & u\in\left(u_{\mathrm{W5}},u_{\mathrm{W6}}\right) \quad (21e)\\ \bar{f}_{\mathrm{W6}}=\bar{k}_{\mathrm{iW}}\dfrac{\left(\frac{1-\beta_{\mathrm{rf}}}{a}u-\beta_{\mathrm{rd}}+\beta_{\mathrm{rf}}\right)\gamma_1}{1-\beta_{\mathrm{rd}}} & u\in\left(u_{\mathrm{W6}},u_{\mathrm{W7}}\right) \quad (21f)\end{cases}$$

where

$$\gamma_1=u_{\mathrm{y}}+a\alpha_{\mathrm{W}}-\alpha_{\mathrm{W}}u_{\mathrm{y}} \quad (22)$$

$$\gamma_2=\left(1-\alpha_{\mathrm{W}}\right)\left(a-u_{\mathrm{y}}\right)-\beta_{\mathrm{uf}}\gamma_1 \quad (23)$$

Thus, we have

$$\begin{aligned}\bar{S}&=\frac{1}{\pi a}\int_0^{2\pi}\bar{f}\sin\theta\mathrm{d}\theta=\frac{1}{\pi a}\int_0^{2\pi}\left(\bar{f}_{\mathrm{H}}+\bar{f}_{\mathrm{S}}+\bar{f}_{\mathrm{W}}\right)\sin\theta\mathrm{d}\theta\\&=\bar{S}_{\mathrm{H}}+\bar{S}_{\mathrm{S}}+\bar{S}_{\mathrm{W}}\end{aligned} \quad (24)$$

$$\begin{aligned}\bar{C}&=\frac{1}{\pi a}\int_0^{2\pi}\bar{f}\cos\theta\mathrm{d}\theta=\frac{1}{\pi a}\int_0^{2\pi}\left(\bar{f}_{\mathrm{H}}+\bar{f}_{\mathrm{S}}+\bar{f}_{\mathrm{W}}\right)\cos\theta\mathrm{d}\theta\\&=\bar{C}_{\mathrm{H}}+\bar{C}_{\mathrm{S}}+\bar{C}_{\mathrm{W}}\end{aligned} \quad (25)$$

4 HARMONIC FREQUENCY RESPONSE OF THE DUAL FRAME-WALL SYSTEM

4.1 Steady-state dynamic response

The steady-state responses of the dual frame-wall system can be evaluated using Eq. (10), which requires calculating $\bar{S}$ and $\bar{C}$ using Eqs. (24) and (25). Fig. 4 presents the responses for different stiffness ratios ($k=\bar{k}_{\mathrm{iH}}:\bar{k}_{\mathrm{iS}}:\bar{k}_{\mathrm{iW}}$) for bilinear, self-centering, and pinching hysteresis systems, where α_{H}, α_{S}, and α_{W} are 0.0, 0.1, and 0.0, respectively and under the same viscous damping of 0.02. When the bilinear system stiffness is low (0.1), as shown in Fig. 4a, the higher self-centering hysteresis causes larger resonance, but the response levels remain at the DC and LS levels for $R_{\mathrm{a}}=0.2$. Since the self-centering hysteresis cannot provide hysteretic damping, the pinching system plays an important role in energy dissipation and reducing resonance. However, when $R_{\mathrm{a}}=0.6$ (Fig. 4b), the response becomes unbounded when the pinching system dominates, making the self-centering building hazardous if the hysteretic damping system deteriorates. After increasing the bilinear system stiffness ratio to 0.5, the resonant responses change significantly. As shown in Fig. 4c, under low excitation intensity ($R_{\mathrm{a}}=0.2$), the peak response for the systems remains around 2.5, despite the different stiffness ratios between the self-centering and pinching systems. Increasing the pinching system stiffness ratio can further decrease the peak value. When $R_{\mathrm{a}}=0.6$ (Fig. 4d), the maximum response increases to approximately 3.6 for $k=0.5:0.5:0.0$. Increasing the stiffness ratio of the pinching system can decrease the peak value. Figs. 4e and 4f compare the steady-state responses of

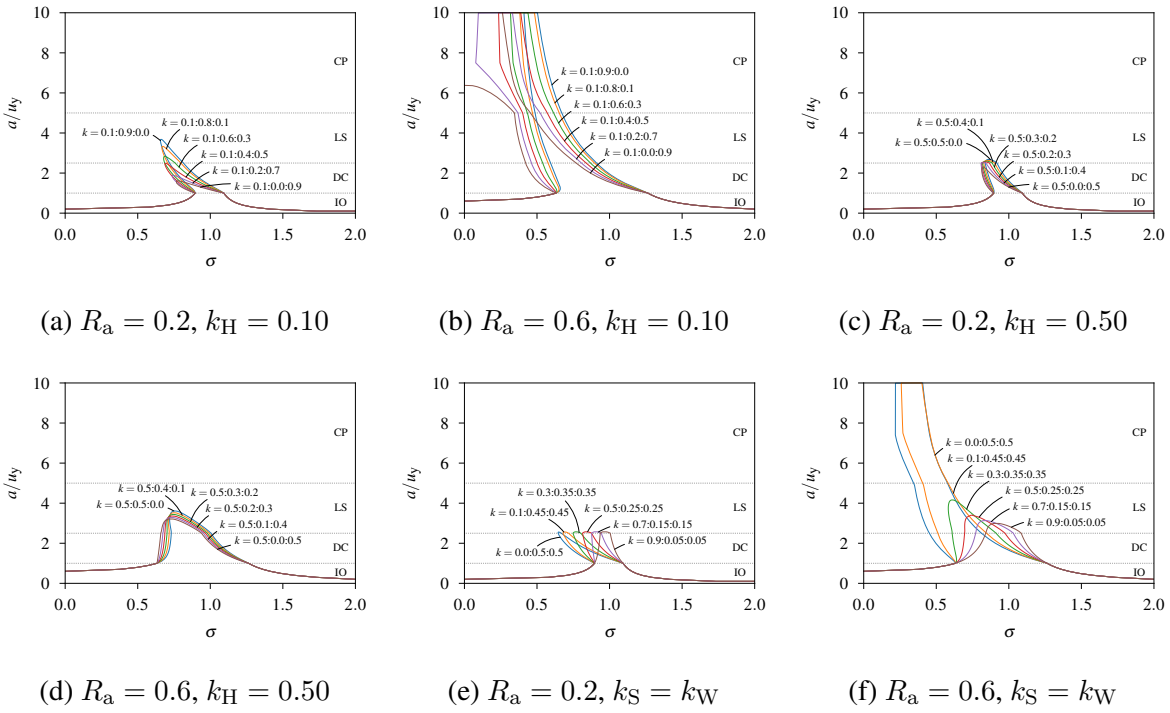

(a) $R_{\mathrm{a}} = 0.2$, $k_{\mathrm{H}} = 0.10$ (b) $R_{\mathrm{a}} = 0.6$, $k_{\mathrm{H}} = 0.10$ (c) $R_{\mathrm{a}} = 0.2$, $k_{\mathrm{H}} = 0.50$

(d) $R_{\mathrm{a}} = 0.6$, $k_{\mathrm{H}} = 0.50$ (e) $R_{\mathrm{a}} = 0.2$, $k_{\mathrm{S}} = k_{\mathrm{W}}$ (f) $R_{\mathrm{a}} = 0.6$, $k_{\mathrm{S}} = k_{\mathrm{W}}$

Figure 4: Steady-state response of dual frame-wall system under different stiffness ratios

systems with the same stiffness ratio of self-centering and pinching systems ($k_{\mathrm{S}} = k_{\mathrm{W}}$) but different stiffness ratios of the bilinear system. Similar to Fig. 4c, the peak response is around 2.5 under low excitation intensity ($R_{\mathrm{a}} = 0.2$), but the higher self-centering and pinching systems bring more nonlinearity and increase the unstable zone. After increasing the excitation intensity ($R_{\mathrm{a}} = 0.6$), the peak responses increase significantly for the system with decreasing bilinear system stiffness (Fig. 4f). Thus, the stiffness ratio between the bilinear, self-centering, and pinching systems controls the dynamic responses of the dual frame-wall system.

The response of dual frame-wall systems with a stiffness ratio of $\bar{k}_{\mathrm{iH}} : \bar{k}_{\mathrm{iS}} : \bar{k}_{\mathrm{iW}} = 0.5 : 0.25 : 0.25$ is presented in Fig. 5, under varying excitation amplitude and damping ratio. Fig. 5a shows that the resonance of the system is initially at the DC level, and then progresses to the LS level as the excitation amplitude increases. At $R_{\mathrm{a}} = 1.0$, the peak response reaches 5.0, indicating that a bilinear system with a stiffness ratio of 0.5 can effectively control the maximum response. Jump phenomena are also observed in these cases. Increasing the damping ratio can significantly decrease the peak response under both low ($R_{\mathrm{a}} = 0.2$, Fig. 5b) and high ($R_{\mathrm{a}} = 0.6$, Fig. 5c) excitation intensities. In the former case, the resonance is brought back to the DC level, where the bilinear system remains elastic, while in the latter case, the viscous damping plays a key role since only half of the bilinear system contributes to the lateral resistance. These results demonstrate that a well-designed dual frame-wall system can exhibit favourable dynamic behaviour.

4.2 Stability analysis

Fig. 6 shows the edges of the solutions of Eq. (16) of the proposed system. In 6a, where $k_{\mathrm{H}} = 0.1$, most of the responses are divided into four zones, corresponding to R_{u} values of 1.0, 2.5, 5.0, and 7.5. Both self-centering and pinching hysteresis have a normalized yielding value of 1.0, and the pinching hysteresis starts to fail at 5.0 and completely fails at 7.5, as shown

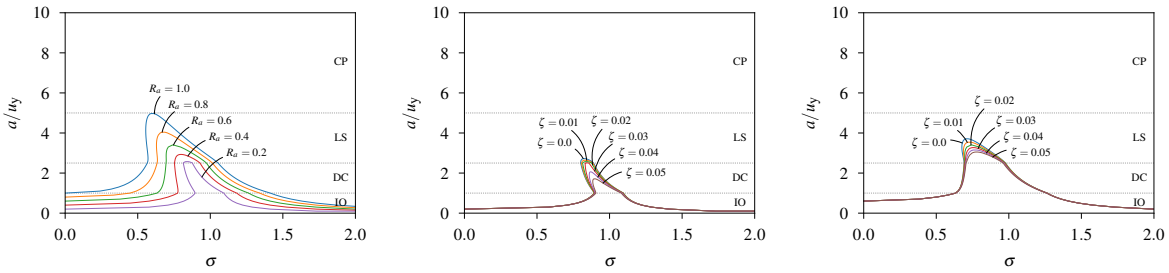

(a) $\zeta = 0.02$ (b) $R_{\mathrm{a}} = 0.2$ (c) $R_{\mathrm{a}} = 0.6$

Figure 5: Steady-state response of dual frame-wall system ($\bar{k}_{\mathrm{iH}} = 0.5$, $\bar{k}_{\mathrm{iS}} = 0.25$, $\bar{k}_{\mathrm{iW}} = 0.25$)

in Figure 2. However, an extra value of 2.5 is contributed from the yielding of the bilinear hysteresis. This indicates that although the stability of the standalone bilinear hysteresis is always stable, the stability behaviour cannot be obtained by summing all the responses in a nonlinear oscillator. For the system where $k = 0.1 : 0.9 : 0.0$ and only bilinear and self-centering hysteresis are combined, the $Q < 0$ zone is bounded and starts at the (1.0,1.0) point and is necking when $R_{\mathrm{u}} = 2.5$. Thus, the corresponding steady-state responses in 4a and 4b are divided into three branches. When $k = 0.1 : 0.8 : 0.1$, pinching hysteresis is introduced, resulting in additional separations of the $Q < 0$ zone at the CP level. However, the pinching system fails at the CP level, bringing a highly nonlinear problem. Further research is required for collapse-prevent behaviour and design. With an increase in the pinching hysteresis, the $Q < 0$ zone shifts to the left, and the area is increased. In the case of $k = 0.1 : 0.1 : 0.9$, the unstable area is unbounded. Therefore, a higher stiffness of the pinching system increases the nonlinearity of the oscillator.

In the results presented in Fig. 6b, it can be seen that as k_{H} is increased to 0.5, the solutions for $Q < 0$ are divided into two zones: a lower zone at the DC level and an upper zone across LS and CP levels. The lower unstable zones are initially formed by the self-centering and pinching hysteresis. By comparing the steady-state responses shown in Figs. 4c and 4d with Fig. 6b, it is apparent that the monotonic decreasing solutions in the steady-state are unstable. The upper zone is bounded at the LS level, but left-bounded at the CP level when $R_{\mathrm{u}} < 7.5$. The bilinear hysteresis contributes to the discontinuity of the zones, and the gap between them is increased with the stiffness of the pinching hysteresis. Fig. 6c presents the overall stability map under different k_{H} values when $k_{\mathrm{S}} = k_{\mathrm{W}}$. When only self-centering and pinching hysteresis are present in the system (i.e., $k = 0.0 : 0.5 : 0.5$), the unstable zone is continuous and left-bounded between $R_{\mathrm{u}} = 5.0$ and $R_{\mathrm{u}} = 7.5$. As k_{H} is increased to 0.1, and $k_{\mathrm{S}} = k_{\mathrm{W}} = 0.45$, necking occurs around $R_{\mathrm{u}} = 2.5$. With further increases in k_{H}, the unstable zone becomes divided. When $k_{\mathrm{H}} = 0.9$, the previous upper unstable zone vanishes. The unstable behaviour of the singular points is, therefore, a result of the self-centering and pinching hysteresis.

6d presents the results of the dual frame-wall system ($k = 0.50 : 0.25 : 0.25$, $\alpha_{\mathrm{H}} = 0.1$) under different viscous damping ratios. The increase in viscous damping does not have a significant effect on the unstable zone at the DC level, where the bilinear system remains elastic and the self-centering and pinching systems behave nonlinearly. However, at the LS and CP levels, it is found that increasing the viscous damping ratio can reduce the unstable zone. The reason for this is mainly due to the coupling of hysteretic damping and viscous damping, as the yielding of a bilinear system provides a large amount of hysteretic damping. However, the exact coupling mechanism remains unclear, and further investigation is needed. The post-yielding

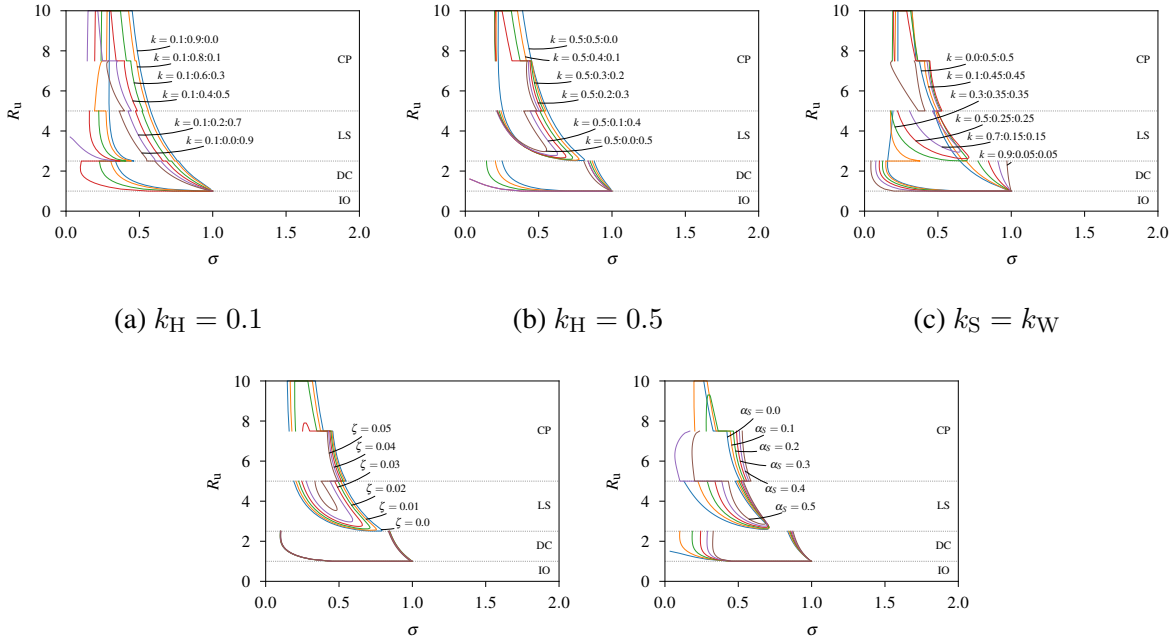

(a) $k_{\mathrm{H}} = 0.1$ (b) $k_{\mathrm{H}} = 0.5$ (c) $k_{\mathrm{S}} = k_{\mathrm{W}}$

(d) $k = 0.50 : 0.25 : 0.25$, $\alpha_H = 0.1$ (e) $k = 0.50 : 0.25 : 0.25$, $\zeta = 0.02$

Figure 6: Stability of dual frame-wall system

stiffness ratio of self-centering hysteresis is an important factor in the nonlinearity of the system. 6e shows the map of $Q < 0$ of the oscillator ($k = 0.50 : 0.25 : 0.25$, $\zeta = 0.02$) under different α_{H}. Increasing the value of α_{H} can shift the unstable zone to the right and decrease its area. Since only 0.25 of self-centering hysteresis is present here, the unstable zone is still able to separate the steady-state responses, leading to the jump phenomenon.

5 CONCLUSIONS

The main focus of this paper is to investigate the nonlinear dynamic behaviour of a mixed dual frame-wall resilient system, comprising of a high-strength moment-resisting steel frame (HS-MRF) and self-centering steel plate shear walls (SC-SPSWs). The hysteretic model employed in this system includes bilinear, self-centering, and pinching hysteresis that represent the HS-MRF, self-centering frame, and steel plate shear wall, respectively. The study utilizes the method of averaging to obtain the analytical solution for a single-degree-of-freedom nonlinear oscillator under harmonic excitation. Based on the analysis, the following conclusions can be drawn.

1. The method of averaging was used to obtain analytical solutions for a single-degree-of-freedom nonlinear oscillator subjected to harmonic excitation and incorporating viscous damping. The stability of the system was also studied by analysing the nature of the singular points. This analysis did not consider any specific hysteresis model, making the solutions applicable to non-time-sensitive nonlinear structural systems.

2. This study on the dual frame-wall system reveals that increasing the proportion of bilinear hysteresis has little impact on resonance but can decrease nonlinearity for lower excitation intensities. However, for higher intensities, an increase in bilinear hysteresis

can notably lower peak responses and reduce both the jump and unbounded phenomena. Most of the unstable responses can be divided into four zones, and the unstable regions are greatly influenced by the ratio of hysteretic models. This steady-state dynamic analysis suggests that a well-designed mix of HS-MRF and SC-SPSW can bring a favourable seismic performance.

ACKNOWLEDGEMENTS

The research described in this paper was financially supported by the National Natural Science Foundation of China (51678474, 52278213), the Natural Science Basic Research Plan in Shaanxi Province of China (2022JM-189), and the China Scholarship Council (202108610187). Any options, findings, conclusions, or recommendations expressed in this publication are those of the authors and do not necessarily reflect the views of the sponsors.

REFERENCES

[1] N. Chancellor, M. Eatherton, D. Roke, and T. Akbaş, "Self-Centering Seismic Lateral Force Resisting Systems: High Performance Structures for the City of Tomorrow," *Buildings*, vol. 4, pp. 520–548, Sept. 2014.

[2] D. Sun, Y. Yang, Y. Ma, Y. Xue, Y. Yu, and S. Feng, "Seismic behavior of self-centering column base with replaceable stiffener angle steels," *Thin-Walled Structures*, vol. 181, p. 110113, Dec. 2022.

[3] S. Feng, Y. Yang, Y. Xue, and Y. Yu, "A post-tensioned hybrid beam-column connection with a web friction device: Experimental study and theoretical analysis," *Journal of Building Engineering*, vol. 43, p. 103105, Nov. 2021.

[4] G. Xu, T. Guo, and A. Li, "Self-Centering Rotational Joints for Seismic Resilient Steel Moment Resisting Frame," *Journal of Structural Engineering*, vol. 149, p. 04022245, Feb. 2023.

[5] C.-C. Chou and J.-H. Chen, "Development of floor slab for steel post-tensioned self-centering moment frames," *Journal of Constructional Steel Research*, vol. 67, pp. 1621–1635, Oct. 2011.

[6] C. Fang, W. Wang, and W. Feng, "Experimental and numerical studies on self-centring beam-to-column connections free from frame expansion," *Engineering Structures*, vol. 198, p. 109526, Nov. 2019.

[7] C. Xie, X. Wang, and G. Vasdravellis, "Mechanical behaviour and experimental evaluation of self-centring steel plate shear walls considering frame-expansion effects," *Journal of Building Engineering*, vol. 72, p. 106636, Aug. 2023.

[8] Y. Zhang and L.-H. Xu, "Cyclic loading tests of a resilient hinged self-centering RC wall," *Engineering Structures*, vol. 270, p. 114920, Nov. 2022.

[9] X. Wang, C. Xie, Z. Jia, and G. Vasdravellis, "Seismic behaviour of post-tensioned beam-to-column connection using slender energy-dissipating rectangles," *Engineering Structures*, vol. 250, p. 113444, Jan. 2022.

[10] P. Mottier, R. Tremblay, and C. Rogers, "Shake table test of a two-story steel building seismically retrofitted using gravity-controlled rocking braced frame system," *Earthquake Engineering & Structural Dynamics*, vol. 50, no. 6, pp. 1576–1594, 2021.

[11] X. Li, F. Zhang, Z. Wang, K. Tian, J. Dong, and L. Jiang, "Shaking table test of a frame structure retrofitted by externally-hung rocking wall with SMA and disc spring self-centering devices," *Engineering Structures*, vol. 240, p. 112422, Aug. 2021.

[12] C. Christopoulos, "Frequency Response of Flag-Shaped Single Degree-of-Freedom Hysteretic Systems," *Journal of Engineering Mechanics*, vol. 130, pp. 894–903, Aug. 2004.

[13] S. Kitayama and C. Yang, "Steady-state dynamic response analysis of self-centering structural systems with viscous damping," *Soil Dynamics and Earthquake Engineering*, vol. 150, p. 106926, Nov. 2021.

[14] F. Hu, G. Shi, and Y. Shi, "Experimental study on seismic behavior of high strength steel frames: Global response," *Engineering Structures*, vol. 131, pp. 163–179, Jan. 2017.

[15] S. Ramhormozian, G. C. Clifton, G. A. MacRae, G. P. Davet, and H.-H. Khoo, "Experimental studies on Belleville springs use in the sliding hinge joint connection," *Journal of Constructional Steel Research*, vol. 159, pp. 81–94, Aug. 2019.

[16] J.-p. Wei, L.-m. Tian, Y. Guo, H.-y. Qiao, Y. Bao, Z.-a. Jiao, and X.-j. Shi, "Numerical study of the seismic performance of a double-hinge steel frame joint," *Journal of Constructional Steel Research*, vol. 187, p. 106963, Dec. 2021.

[17] A.-L. Zhang, X. Chen, Z.-Q. Jiang, Y.-T. Kang, and X.-F. Yang, "Experiment on seismic behavior of earthquake-resilience prefabricated cross hinge column foot joint," *Journal of Constructional Steel Research*, vol. 189, p. 107056, Feb. 2022.

[18] A. I. Dimopoulos, T. L. Karavasilis, G. Vasdravellis, and B. Uy, "Seismic design, modelling and assessment of self-centering steel frames using post-tensioned connections with web hourglass shape pins," *Bulletin of Earthquake Engineering*, vol. 11, pp. 1797–1816, Oct. 2013.

[19] A. S. Tzimas, A. I. Dimopoulos, and T. L. Karavasilis, "EC8-based seismic design and assessment of self-centering post-tensioned steel frames with viscous dampers," *Journal of Constructional Steel Research*, vol. 105, pp. 60–73, Feb. 2015.

[20] X. Huang, Z. Zhou, Q. Xie, R. Xue, and D. Zhu, "Force distribution analysis of self-centering coupled-beams for moment-resisting-frames without floor elongation," *Engineering Structures*, vol. 147, pp. 328–344, Sept. 2017.

[21] X. Guan, H. Burton, and S. Moradi, "Seismic performance of a self-centering steel moment frame building: From component-level modeling to economic loss assessment," *Journal of Constructional Steel Research*, vol. 150, pp. 129–140, Nov. 2018.

[22] P. M. Clayton, T. B. Winkley, J. W. Berman, and L. N. Lowes, "Experimental Investigation of Self-Centering Steel Plate Shear Walls," *Journal of Structural Engineering*, vol. 138, pp. 952–960, July 2012.

[23] M. Dastfan and R. Driver, "Test of a Steel Plate Shear Wall with Partially Encased Composite Columns and RBS Frame Connections," *Journal of Structural Engineering*, vol. 144, p. 04017187, Feb. 2018.

[24] J. Yu, J. Huang, B. Li, and X. Feng, "Experimental study on steel plate shear walls with novel plate-frame connection," *Journal of Constructional Steel Research*, vol. 180, p. 106601, May 2021.

[25] Y. Shi, Z. Luo, Y. Xu, Y. Zou, L. Xu, and Q. Ma, "Experimental study on the seismic behavior of high-performance cold-formed steel plate shear walls," *Engineering Structures*, vol. 251, p. 113552, Jan. 2022.

[26] L. N. Lowes, N. Mitra, and A. Altoontash, "A Beam-Column Joint Model for Simulating the Earthquake Response of Reinforced Concrete Frames," Technical Report PEER Report 2003-10, Pacific Earthquake Engineering Research Center, University of California, Berkeley, CA., Feb. 2003.

[27] F. McKenna, M. H. Scott, and G. L. Fenves, "Nonlinear Finite-Element Analysis Software Architecture Using Object Composition," *Journal of Computing in Civil Engineering*, vol. 24, pp. 95–107, Jan. 2010.

[28] A. H. Nayfeh and D. T. Mook, *Nonlinear Oscillations (Pure and Applied Mathematics: A Wiley - Interscience Series of Texts, Monographs and Tracts)*. New York: John Wiley & Sons, 1979.